Single/Three-Phase Compatible Sigma-Type OBC With Reduced Electrolytic Capacitor Volume

Jaehoon Kim, Donghan Lee, Chaeyoung Suk, Gibum Yu, *Graduate Student Member, IEEE*, and Sewan Choi, *Fellow, IEEE*

***Abstract*—This article proposes a sigma-type dc–dc converter with a reduced energy volume of the electrolytic capacitor (E-cap) for single- and three-phase compatible on-board charger (OBC). The proposed relay box configuration uses a minimal number of relays. In single-phase grid, the E-cap is connected to the dc-link via the input-parallel output-series (IPOS) structure to absorb second harmonic current. In a three-phase grid, a film capacitor connects to the dc-link instead of E-cap, maintaining the low voltage rating of the E-cap by the input-independent output-series (IIOS) structure. Additionally, the power of the regulated converter is reduced, allowing most of the power to flow through the unregulated converter, achieving high efficiency. The proposed sigma converter achieves soft-switching under a wide voltage range and reduces the power burden of the regulated converter through a reconfigurable leg. Experimental results from an 11 kW prototype validate the proposed circuit. The converter achieved a peak efficiency of 98.12% and maintained high efficiency under a wide voltage range.**

***Index Terms*—Bidirectional on-board charger (OBC), electric vehicle (EV), high efficiency, sigma dc–dc converter, universal charger, wide voltage range.**

I. Introduction

RECENTLY, the rising fuel costs and concerns over air pollution have led to an increasing interest in electric vehicles (EVs) [1]. According to the Global EV Outlook 2024, approximately 14 million electric vehicles were sold worldwide in 2023, accounting for 18% of total vehicle sales. Additionally, by 2035, it is anticipated that electric vehicles will make up two-thirds of all vehicles, potentially reducing oil consumption by 12 million barrels [2]. In electric vehicles, the on-board charger (OBC) is one of the key components for charging high-voltage battery from single-phase or three-phase ac grids. Recently, there has been a trend of increasing battery capacity to extend driving range. To reduce charging time, single-phase OBCs typically provide a charging capacity of 7.4 kW, while three-phase OBCs offer charging capacities ranging from 11 to 22 kW [3]. In North America, single-phase OBCs are used. However, in Europe and Asia, both single-phase and three-phase systems are used. In particular, three-phase charging infrastructure is dominant in European countries where many EVs are equipped with three-phase OBCs [4], [5]. Compared to single-phase OBCs, three-phase OBCs can reduce charging time by approximately 66% due to their higher charging power [6]. Therefore, developing OBCs that support both single-phase and three-phase operation is valuable for commercial and consumer convenience. Single-phase and three-phase compatible OBCs are classified into modular and non-modular types. Currently, the modular three-phase structure, which uses three isolated ac–dc converters, is widely used. The modular type offers easy power scalability and potentially lower manufacturing costs, but it has the disadvantage of a higher number of components due to its modular structure [7], [8], [9], [10], [11], [12]. On the other hand, the non-modular two-stage type has the advantage of fewer components compared to the modular type. However, it requires a large E-cap for single-phase and three-phase compatible operation. When operating with a single-phase grid, the dc-link capacitor typically has 400 V applied to it and requires significant capacitance to absorb the second harmonic current [13], [14], [15], [16]. In a 7.4 kW system, approximately 3 mF is needed to maintain the dc-link voltage ripple. In contrast, for a three-phase OBC, although a higher voltage of 800 V is required, a much smaller capacitance is sufficient to achieve the same voltage ripple as in a single-phase OBC [17]. Therefore, a small film capacitor can be applied in three-phase OBCs. However, to ensure compatibility with both single-phase and three-phase grids, the dc-link capacitor must be rated for voltages above 800 V and have a large capacitance of approximately 3 mF, which is a notable disadvantage. Table I compares the required dc-link capacitors based on per-unit calculations by OBC type. It should be noted that for single-phase and three-phase compatible inputs, the capacitor energy volume is four

Received 4 June 2024; revised 24 September 2024; accepted 27 October 2024. *(Corresponding author: Sewan Choi.)*

Jaehoon Kim and Sewan Choi are with the Department of Electrical and Information Engineering, Seoul National University of Science and Technology, Seoul 01811, South Korea (e-mail: habak@seoultech.ac.kr; schoi@seoultech.ac.kr).

Donghan Lee is with the Department of New and Renewable Energy Convergence, Seoul National University of Science and Technology, Seoul 01811, South Korea (e-mail: donghan@seoultech.ac.kr).

Chaeyoung Suk is with the Department of Converter Development Project, LG Magna, Incheon 22744, South Korea (e-mail: chaeyoung11.suk@lgmagna.com).

Gibum Yu is with the Bradley Department of Electrical and Computer Engineering, Center for Power Electronics Systems (CPES), Virginia Polytechnic and State University, Blacksburg, VA 24061, USA (e-mail: gibumyu@vt.edu).

Digital Object Identifier 10.1109/TIE.2024.3493166

TABLE I
COMPARISON OF REQUIRED DC-LINK CAPACITOR'S ENERGY VOLUME IN DIFFERENT GRID TYPES OF OBC [$V_{DC,Link}$ = 400 V (1P.U.), $C_{DC,Link}$ = 3 MF (1P.U.)]

OBC Type	Single-phase	Three-phase	Single-and three-phase compatible
	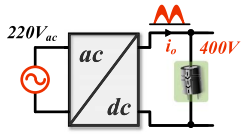	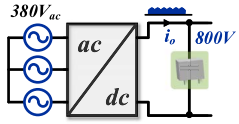	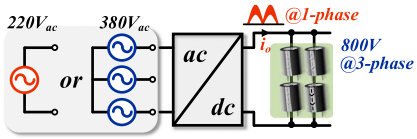
$V_{DC,Link}$	1 p.u.	2 p.u.	2 p.u. (at three-phase)
$C_{DC,Link}$	1 p.u.	0.167 p.u.	1 p.u. (at single-phase)
Energy volume	0.5 p.u.	0.334 p.u.	2 p.u.

times greater than that of single-phase OBCs [18]. This article proposes a non-modular sigma-type dc–dc converter compatible with both single-phase and three-phase grids. Through circuit integration, the number of components has been minimized, and a direct-current transformer (DCX)-based sigma converter has been applied to enhance efficiency [19], [20], [21], [22]. Additionally, the proposed relay structure in the dc-link stage reduces the energy volume of the E-caps.

II. PROPOSED SIGMA-TYPE STRUCTURE FOR SINGLE- AND THREE-PHASE COMPATIBLE OBC

In this section, three connection methods are introduced for reducing the voltage rating of the dc-link capacitor and/or converter modules of the single- and three-phase compatible OBC, as shown in Table II. In the relay box, relay *1-p* closes for single-phase input, while relay *3-p* closes for three-phase input. With the connection method 1, in single-phase operation, the dc-link capacitors are connected in parallel, and the converters are also connected in parallel. Therefore, dc-link capacitor has a voltage rating of 400 V and sufficient capacitance to absorb the second harmonic current. However, in three-phase mode, operation is not possible due to the input-series output-series (ISOS) connection of the upper and lower modules [23]. Method 2 illustrates the circuit by changing only the dc-link capacitor connection method. As shown Table II, the voltage rating of the dc-link capacitor in both single-phase and three-phase modes can be 400 V, the same as method 1. Additionally, the connection of the converter module is input-parallel output-series (IPOS) in both grid modes, so there are no regulation issues, unlike the three-phase operation of method 1. However, since the converter modules are connected in parallel in the three-phase mode, the voltage rating of the dc-link side switches is 800 V. To lower the voltage rating of the electrolytic capacitor and converter module, the relay box can be configured as in the proposed method. For high capacitance in single-phase operation, the upper unregulated converter and regulated converter are configured in parallel with the dc-link capacitor. In three-phase operation, the E-cap and the output capacitor of the regulated converter are connected in series. This configuration results in the upper converter and the lower two-stage converter being composed of an input-independent output-series (IIOS) structure [24]. This arrangement enables regulation while lowering the voltage rating of the E-cap. In conclusion, by using the proposed relay connection method depicted in

TABLE II
PROPOSED CONNECTIONS OF SIGMA TYPE CONVERTER FOR SINGLE-/THREE- PHASE COMPATIBLE OBC

※ Unregulated converter : U, Regulated converter : R

	Single- and Three- phase compatible OBC Structure	
	Single-phase operation	Three-phase operation
Method 1	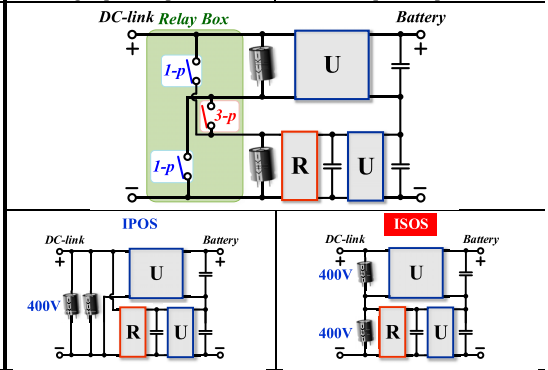	
Method 2	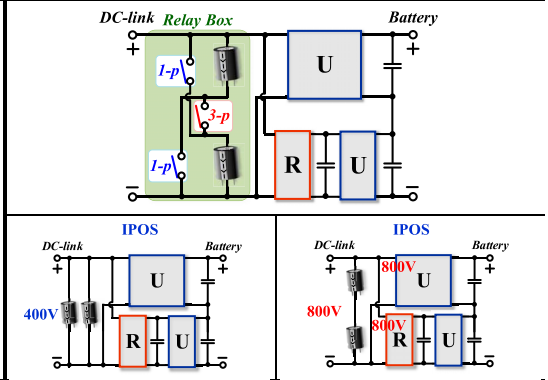	
Proposed Method	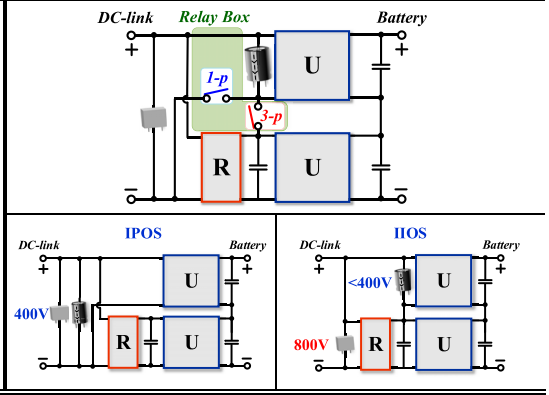	

Table II, the OBC can operate in both single-phase and three-phase compatible systems, allowing for a reduction in the rated voltage of the electrolytic capacitor for the dc-link capacitor.

A. Consideration for a Single-Phase and Three-Phase Compatible Sigma-Type OBC

In on-board charger application, all converter modules should be isolated, and several conditions should be considered to optimize performance and components.

1) The rated voltage of the switches must be considered. In a three-phase grid input, the dc-link voltage should be greater than 600 V. Therefore, it is advisable to connect the converter modules on the dc-link side in series to reduce the number of high-voltage rated switches.
2) The volume of the electrolytic capacitor need to be reduced. During single-phase grid connection, the dc-link capacitor should absorb the second harmonic current, requiring a large capacitance with a 450 V voltage rating. However, in three-phase grid connection, the required capacitance is smaller, but the rated voltage must be above 800 V. Therefore, in a non-modular two-stage structure, a considerable number of electrolytic capacitors are generally needed to satisfy both single-phase and three-phase operations.
3) The sigma structure is generally vulnerable to wide battery voltage range operation. Since the maximum power rating of each converter increases in the wide voltage range, an over-rating design is required. Therefore, a structure and control technique that are advantageous over a wide voltage range are necessary.
4) Achieving soft-switching under a wide voltage range is important for high efficiency, high power density, and low electromagnetic interference (EMI) noise. In conclusion, these four factors should be considered to achieve high power and efficiency in a non-modular two-stage OBC.

B. Proposed Structure

Table III briefly outlines the proposed OBC structure depending on the grid condition. The proposed sigma converter is constructed using two series-resonant converter (SRC) converters with DCX operation for the unregulated converter and one regulated converter. For single-phase charging, the relay for single-phase operation is turned on as per the circuit scheme. Thus, the inputs of DCX1 and the regulated converter are connected in parallel, with the regulated power P_2 flowing to the regulated converter + DCX2, and the unregulated power P_1 flowing to DCX1. In this scenario, the voltage rating of the dc-link capacitor is 400 V, and the film capacitor, which is connected closely to the regulated converter, is parallel-connected with the electrolytic capacitor. In three-phase mode, the relay for three-phase operation is turned on, enabling the series input connection of DCX1 and DCX2, while the input of the regulated converter is connected in parallel with the output of the ac–dc part. The unregulated converters operate as resonant converters capable of DCX operation, theoretically having no switching losses. In contrast, the regulated converter incurs significant turn-OFF losses, underscoring the importance of reducing the rated power of regulated converters. Fortunately,

TABLE III
OPERATION OF PROPOSED SINGLE/THREE-PHASE COMPATIBLE SIGMA TYPE OBC

	Single-phase operation	Three-phase operation
Circuit Scheme	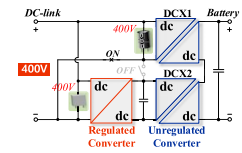	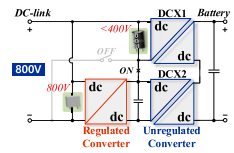
Power flow	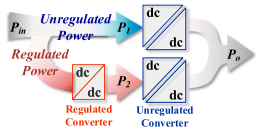	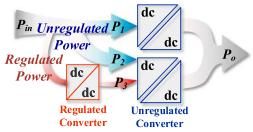
DC-link Capacitor	Electrolytic Capacitor (450V, High capacitance) + Film Capacitor (800V, Low capacitance)	Film Capacitor (800V, Low capacitance)

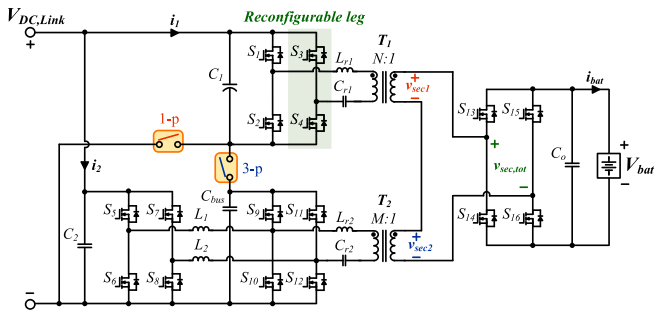

Fig. 1. Circuit configuration of the proposed sigma type OBC.

in three-phase operation, the power of DCX2 is the sum of regulated power P_3 and unregulated power P_2, resulting in reduced regulated power P_3 compared to single-phase operation. Consequently, the burden on the regulated converter can be further reduced in three-phase mode. Moreover, the voltage rating of the electrolytic capacitor can be maintained at 400 V, and low-capacitance film capacitors can be used for the dc-link capacitor. Therefore, there is no requirement to increase the rated voltage of the electrolytic capacitor, resulting in a smaller volume for the electrolytic capacitor.

III. CIRCUIT CHARACTERISTIC OF PROPOSED SIGMA CONVERTER

A. Circuit Configuration

The proposed converter is shown in Fig. 1 and consists of two types of converters. One is the unregulated converter for DCX operation, and the other is the regulated converter for regulating the entire charger. And two relays are configured to convert single-phase and three-phase operation modes, which are covered in the Section IV. The unregulated converter for DCX operation is commonly implemented using the SRC, which is popular for bidirectional operation. Unlike the frequency-controlled CLLLC converter, which does not operate at the load-independent point, DCX-SRC operates only at the load-independent point, involving only the resonant inductor L_r and resonant capacitor C_r in the

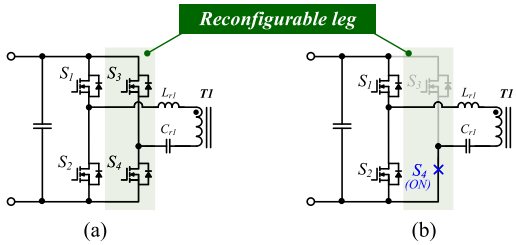

Fig. 2. Reconfigurable leg for wide voltage range operation. (a) Full-bridge mode. (b) Half-bridge mode.

resonant loop. Thus, there is no requirement for complex design of L_r and magnetizing inductor L_m to satisfy voltage gain. This facilitates the use of leakage inductance inherent in the transformer as the resonant inductor. Meanwhile, since the SRC used as an unregulated converter operates as DCX, it suffers from the drawback of consistently producing the same output voltage when the input voltage is fixed. However, in the case where the primary side is configured as a full-bridge, as depicted in Fig. 2, the output voltage of the SRC converter can be adjusted using the topology morphing technique by toggling the switches of the reconfigurable leg. Fig. 2(a) shows the operation of a typical full-bridge structure, where all switches operate with 0.5 duty cycle. In this mode, the output voltage of DCX1 is V_{C1}/N, which represents the input voltage multiplied by the turn ratio. Fig. 2(b) depicts the operation of a half-bridge structure using topology morphing technique. During this process, S_3 remains turned off while S_4 remains turned on. Therefore, it becomes a half-bridge structure in which only the S_1 and S_2 legs operate with a duty cycle of 0.5. When operating in half-bridge mode, the output voltage of the DCX1 becomes $V_{C1}/2N$, which is half of the input voltage multiplied by the turn ratio. Therefore, when applying the reconfigurable leg to OBC applications where the dc-link voltage is fixed, it can be utilized as a half-bridge structure when the battery voltage is low and as a full-bridge structure when the battery voltage is high. Consequently, the regulated converter operates within a narrower voltage regulation range, enhancing the overall converter design for improved efficiency. The lower side of the proposed converter, as shown in Fig. 3, consists of a converter integrating the buck–boost converter and DCX-SRC proposed in [25], [26]. The SRC converter operates at its resonant frequency without any control, while the buck–boost converter regulates the output voltage and current through duty control of bridge 1, similar to a conventional cascaded buck–boost converter. It achieves ZVS turn-ON of each switch through phase-shift control of bridge 1 and bridge 2 [27], [28], [29], [30]. All switches in the integrated converter not only achieve soft-switching, but also the buck–boost inductor current and resonant current cancel each other out in the integrated leg of bridge 2 and bridge 3, resulting in reduced conduction losses. With these characteristics, the buck–boost integrated DCX-SRC can be considered suitable for isolated converters requiring high-frequency operation and high efficiency. Fig. 4(a) depicts the conventional secondary side circuit configuration, where the secondary bridges of DCX1 and DCX2 are connected in series. When DCX1 and DCX2 operate at the same switching frequency and phase, as shown in Fig. 4(b), only one bridge can be used, and the secondary sides of transformers T_1 and T_2 are connected is series.

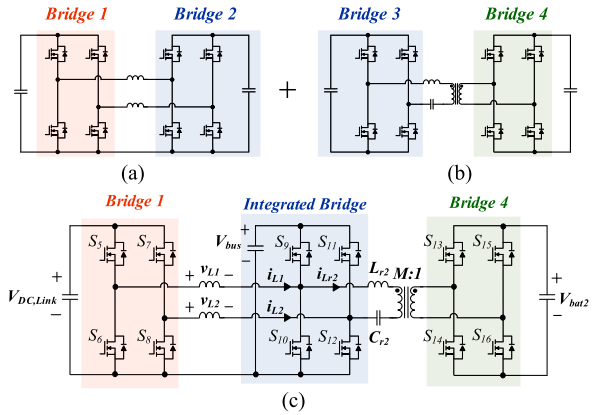

Fig. 3. Regulated converter + DCX-SRC circuit. (a) Cascaded buck–boost converter. (b) DCX-SRC converter. (c) Buck–boost integrated DCX-SRC.

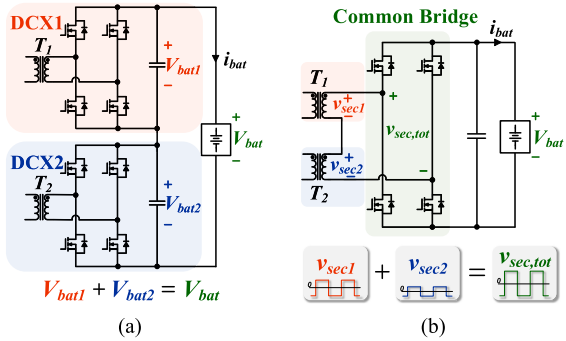

Fig. 4. Secondary-side circuit configuration. (a) Series connection circuit of DCX1, DCX2 secondary. (b) Common bridge secondary circuit.

B. Operating Principles

In this section, only the operating principles of the lower-side buck–boost integrated DCX-SRC2 are discussed, as the upper-side SRC is simply in DCX operation. First, the switching frequency of all switches in the converter is fixed to the resonant frequency of the SRC. The switches S_5–S_8 operate with a duty cycle of D and $1\text{-}D$, while switches S_9–S_{16} maintain a fixed 0.5 duty. Hence, based on the voltage-second balance principle of the filter inductor L_1, there is as follows:

$$D \cdot V_{\mathrm{DC,Link}} = 0.5 V_{\mathrm{Bus}}. \tag{1}$$

And, since SRC2 operates in DCX mode at the resonant frequency, the voltage gain of SRC2 can be expressed as M, where M is the turn ratio of transformer T_2

$$\frac{V_{\mathrm{bat2}}}{V_{\mathrm{bus}}} = \frac{1}{M}. \tag{2}$$

Through the two equations above, the overall voltage transfer ratio of the buck–boost integrated DCX-SRC2 is as follows:

$$\frac{V_{\mathrm{bat2}}}{V_{\mathrm{DC,Link}}} = \frac{2D}{M}. \tag{3}$$

Fig. 5 illustrates the key waveforms of the regulated part of the proposed converter. Switches S_5 and S_6 operate complementarily with duty cycles of D and $1\text{-}D$, respectively, to perform duty control. In addition, switches S_9–S_{10} and S_{13}–S_{14} operate

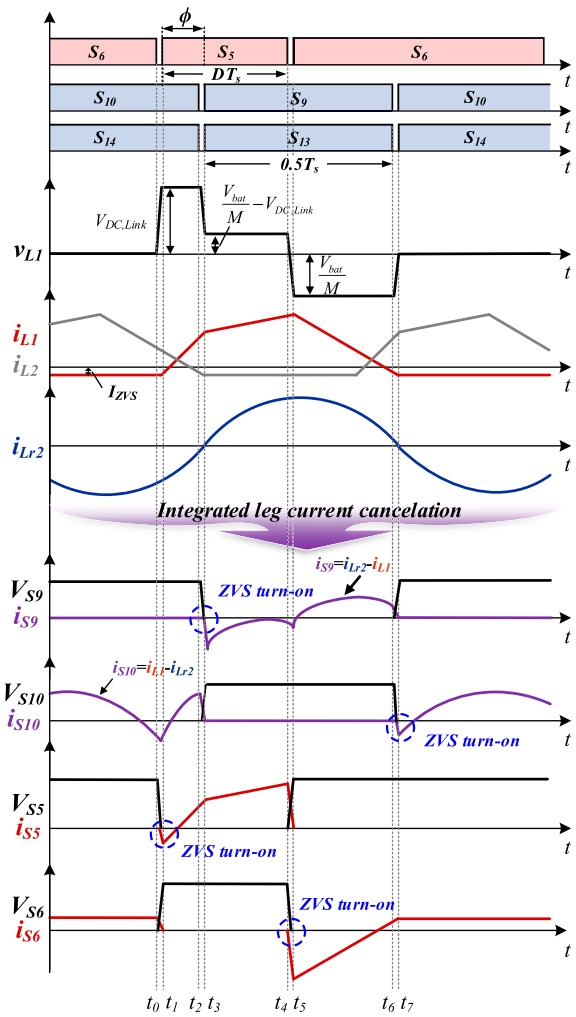

Fig. 5. Key waveform of regulated converter + DCX-SRC2 converter.

with a fixed 0.5 duty for DCX-SRC operation. Since DCX2 operates at a fixed duty and frequency at resonant point, a resonant sinusoidal current flows through L_{r2}, assuming that L_m is sufficiently large. By adjusting the phase-shift angle Φ between S_5 and S_9, the voltage applied to v_{L1} can be modulated, which allows the adjustment of the i_{L1} current magnitude at t_1, t_3, t_5, and t_7. The ZVS conditions for the primary-side switches of the regulated converter, as shown in Table IV, demonstrate that ZVS turn-ON for S_5, S_6 and S_9, S_{10} can be achieved through adjustment of i_{L1} via the phase-shift angle Φ. Additionally, in conventional DCX-SRC, the resonant current i_{Lr2} flows through switches S_9 and S_{10}. However, in the buck–boost integrated DCX-SRC structure, current cancellation occurs, and only the difference between the resonant current i_{Lr2} and the buck–boost inductor current i_{L1} flows through the switches [25], [26].

IV. Operating of Single Phase and Three Phase

Section III covered the operation of the lower-side regulated converter. This chapter describes relay operations and controllers for single-phase and three-phase compatibility. It also discusses the design guidelines for transformer turn ratios to achieve optimal operation.

TABLE IV
ZVS Conditions of the Regulated Converter

Bridge 1		*Integrated Bridge*	
S_5	$i_{L1} < 0$	S_9	i_{Lr2}-$i_{L1} < 0$
S_6	$i_{L1} > 0$	S_{10}	i_{L1}-$i_{Lr2} < 0$

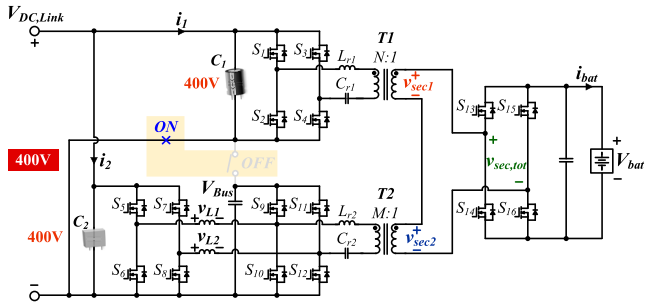

Fig. 6. Circuit configuration for single-phase grid.

A. Operating Principles for Single-Phase Grid Connection

Fig. 6 illustrates the converter structure when a single-phase grid is input. In this configuration, Relay *1-p* is in the on-state while relay *3-p* is off, and the input voltage $V_{\mathrm{DC,Link}}$ is connected in parallel to the upper and lower modules. Therefore, the input capacitor of DCX-SRC1 C_1, and the input capacitor of the regulated converter C_2, are connected in parallel. In a single-phase grid input, the PFC converter regulates the output voltage to 400 V. Hence, the rating of the electrolytic capacitor C_1, intended to absorb low-frequency ripple, could be selected as 450 V. When the battery voltage is low, the reconfigurable leg operates in a half-bridge structure. The relationship between the output voltages of the upper and lower converters is as follows:

$$|V_{\mathrm{sec1}}| = \frac{V_{\mathrm{DC,Link}}}{2N} \tag{4}$$

$$|V_{\mathrm{sec2}}| = |V_{\mathrm{sec2,tot}}| - |V_{\mathrm{sec1}}| = V_{\mathrm{bat}} - \frac{V_{\mathrm{DC,Link}}}{2N}. \tag{5}$$

Therefore, the input voltage of DCX-SRC2, V_{bus}, is as follows:

$$V_{\mathrm{bus}} = M \cdot \left(V_{\mathrm{bat}} - \frac{V_{\mathrm{DC,Link}}}{2N} \right). \tag{6}$$

From (1) and (6), the duty cycle of regulated converter is as follows:

$$D = \frac{M \cdot \left(V_{\mathrm{bat}} - \frac{V_{\mathrm{DC,Link}}}{2N} \right)}{2V_{\mathrm{DC,Link}}}. \tag{7}$$

In single-phase grid mode, the rated power of each converter is proportional to the output voltage of each converter. Since the secondary side has a series structure, the current flowing through the secondary side of DCX1 and DCX2 is identical, resulting in power being shared in proportion to V_{sec1} and V_{sec2}. Using the equations mentioned above, the upper unregulated power P_1 and lower regulated power P_2 in the single-phase structure

outlined in Table III can be expressed as follows:

$$P_1 = \frac{V_{\mathrm{DC,Link}}}{2N} \cdot I_{\mathrm{bat}} \tag{8}$$

$$P_2 = \left(V_{\mathrm{bat}} - \frac{V_{\mathrm{DC,Link}}}{2N}\right) \cdot I_{\mathrm{bat}}. \tag{9}$$

When the battery voltage is high, the reconfigurable leg operates in a full-bridge structure, and the relationship between the output voltages of the upper and lower converters is as follows:

$$|V_{\mathrm{sec1}}| = \frac{V_{\mathrm{DC,Link}}}{N} \tag{10}$$

$$|V_{\mathrm{sec2}}| = |V_{\mathrm{sec2,tot}}| - |V_{\mathrm{sec1}}| = V_{\mathrm{bat}} - \frac{V_{\mathrm{DC,Link}}}{N}. \tag{11}$$

Therefore, the input voltage of DCX-SRC2, V_{bus}, is as follows:

$$V_{\mathrm{bus}} = M \cdot \left(V_{\mathrm{bat}} - \frac{V_{\mathrm{DC,Link}}}{N}\right). \tag{12}$$

From (1) and (12), the duty cycle of regulated converter is as follows:

$$D = \frac{M \cdot \left(V_{\mathrm{bat}} - \frac{V_{\mathrm{DC,Link}}}{N}\right)}{2V_{\mathrm{DC,Link}}}. \tag{13}$$

In this mode, unregulated power P_1 and regulated power P_2 can be expressed as follows:

$$P_1 = \frac{V_{\mathrm{DC,Link}}}{N} \cdot I_{\mathrm{bat}} \tag{14}$$

$$P_2 = \left(V_{\mathrm{bat}} - \frac{V_{\mathrm{DC,Link}}}{N}\right) \cdot I_{\mathrm{bat}}. \tag{15}$$

B. Operating Principles for Three-Phase Grid Connection

Fig. 7 shows the converter structure when inputting a three-phase grid, with relay *1-p* in the OFF state and relay *3-p* in the ON state. In this scenario, C_1 and C_{bus} are connected in series, while the input of the regulated converter is connected in parallel with the dc-link

$$V_{\mathrm{DC,Link}} = V_{C1} + V_{\mathrm{bus}}. \tag{16}$$

In three-phase grid mode, there is no low-frequency ripple component in the dc-link capacitor, unlike in single-phase grid mode. Through this structure, the electrolytic capacitor C_1 can maintain the same low voltage rating as with single-phase grid input, and a film capacitor C_2, which has a low capacitance, is used as the dc-link capacitor. Even in three-phase grid mode, the reconfigurable leg operates in a half-bridge structure in low battery voltage situations. From (1), the output voltage of DCX-SRC2 is as follows:

$$|V_{\mathrm{sec2}}| = \frac{2D \cdot V_{\mathrm{DC,Link}}}{M}. \tag{17}$$

Therefore, the output voltage of DCX-SRC1 is as follows:

$$|V_{\mathrm{sec1}}| = V_{\mathrm{bat}} - |V_{\mathrm{sec2}}| = V_{\mathrm{bat}} - \frac{2D \cdot V_{\mathrm{DC,Link}}}{M}. \tag{18}$$

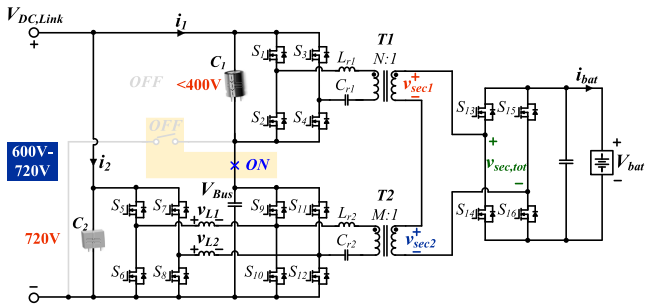

Fig. 7. Circuit configuration for three-phase grid.

Since reconfigurable leg is a half-bridge structure, V_{C1} reflects twice the turn ratio N, as follows:

$$V_{C1} = \frac{2N \cdot (M \cdot V_{\mathrm{bat}} - 2D \cdot V_{\mathrm{DC,Link}})}{M}. \tag{19}$$

Duty cycle is obtained from (1), (16), and (19) as follows:

$$D = \frac{M \cdot (V_{\mathrm{DC,Link}} - 2N \cdot V_{\mathrm{bat}})}{2V_{\mathrm{DC,Link}} \cdot (M - 2N)}. \tag{20}$$

In three-phase grid mode, the unregulated power also flows through DCX-SRC2 via relay *3-p*. Therefore, during three-phase operation, the regulated converter bears only a portion of the power flowing through DCX-SRC2. The rated power of each converter is as follows:

$$P_{\mathrm{DCX1}} = P_1 = \left(V_{\mathrm{bat}} - \frac{2\mathrm{D} \cdot V_{\mathrm{DC,Link}}}{M}\right) \cdot I_{\mathrm{bat}} \tag{21}$$

$$P_{\mathrm{DCX2}} = P_2 + P_3 = \frac{2D \cdot V_{\mathrm{DC,Link}}}{M} \cdot I_{\mathrm{bat}} \tag{22}$$

$$P_{\mathrm{Regulated}} = P_3 = V_{\mathrm{DC,Link}} \cdot \left(\frac{V_{\mathrm{bat}} \cdot I_{\mathrm{bat}}}{V_{\mathrm{DC,Link}}} - \frac{P_1}{V_{C1}}\right). \tag{23}$$

When the battery voltage is high, the same as in single-phase mode, the reconfigurable leg operates in a full-bridge configuration. Consequently, the voltage across C_1 reflects the turn ratio N, as follows:

$$V_{C1} = \frac{N \cdot (M \cdot V_{\mathrm{bat}} - 2D \cdot V_{\mathrm{DC,Link}})}{M}. \tag{24}$$

Duty cycle is obtained from (1), (16), and (24) as follows:

$$D = \frac{M \cdot (V_{\mathrm{DC,Link}} - N \cdot V_{\mathrm{bat}})}{2V_{\mathrm{DC,Link}} \cdot (M - N)}. \tag{25}$$

And the rated power of each converter is same as (21)–(23). Fig. 8 shows the control block diagram of the proposed sigma converter. The battery current and voltage controls are achieved by adjusting the duty cycles of S_5~S_8. S_5 and S_6, along with S_7 and S_8, operate with a 180° phase shift, thereby achieving interleaving effects. To balance the currents through the inductors L_1 and L_2 of each phase, a $D_{\mathrm{bal.}}$ is added. The previously obtained duty cycle equation can be used as a feed-forward term D_{ff} in duty control. Meanwhile, to accommodate a wide range of battery voltages, a

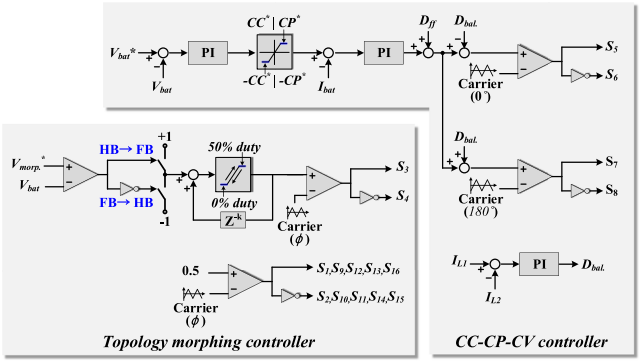

Fig. 8. Control block diagram of proposed converter.

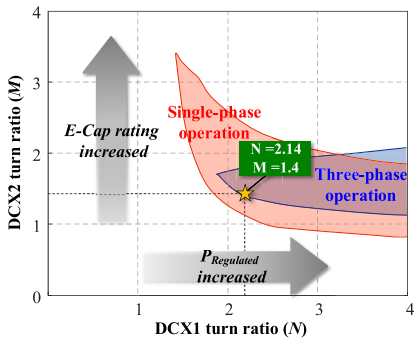

Fig. 9. Available turn ratio combination of DCX converters.

morphing controller is implemented. When the battery voltage exceeds the set morphing voltage, the duty cycle of S_3 gradually increases from 0% to 50%, transitioning to full-bridge operation. Conversely, if the battery voltage drops below the morphing voltage, the duty cycle of S_3 decreases from 50% to 0%, transitioning to half-bridge operation. As a result, the operational duty range of the regulated converter can be reduced.

C. Optimal Design of Transformer Turn Ratio

Fig. 9 illustrates the available transformer turn ratios N and M for single-phase and three-phase operation, respectively. Considering the parasitic resistance component and duty margin, the duty range is limited to 0.2–0.8, and the turn ratio combination that can operate across the entire battery voltage range is selected from the overlapping area of the single-phase and three-phase operation. During single-phase operation, as the turn ratio N of the upper DCX1 increases, V_{sec2} increases, thereby increasing the power burden on the regulated converter. Therefore, using a smaller N is more efficient. On the other hand, increasing the turn ratio M of the lower DCX2 can reduce the power burden on the regulated converter during three-phase operation. However, this comes with the trade-off of an increased voltage rating for the electrolytic capacitor. Considering these factors, N is selected as 2.14 and M as 1.4. Using the selected turn ratios, the power ratio of the regulated converter K_r for different battery voltages according to the grid input is shown in Fig. 10. Above a 330 V battery voltage (V_{morp}), the regulated power decreases through topology morphing. This is particularly evident

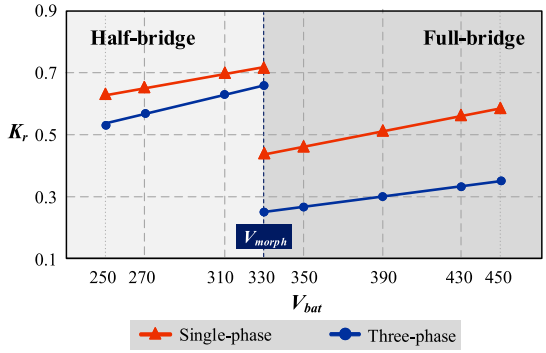

Fig. 10. Relationship between the regulated converter's power and the total power ($K_r = P_{reg}/P_{tot}$).

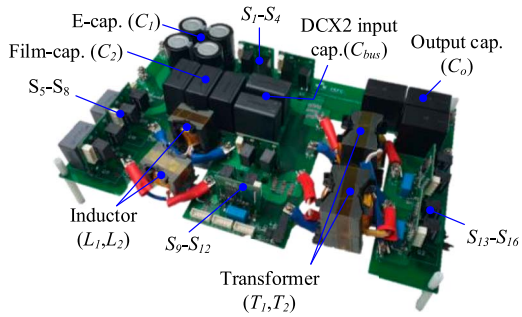

Fig. 11. Prototype of the proposed 11 kW sigma converter.

TABLE V
COMPONENTS RATINGS AND DESIGN PARAMETERS

Components		Values
Switches	S_1∼S_4, S_9∼S_{12}	NTHL060N090SC1 (ST) 650 V/45 mOhm
	S_5∼S_8	SCTWA35N65G2V (Onsemi) 900 V/60 mOhm
	S_{13}∼S_{16}	SCTW100N65G2AG (ST) 650 V/20 mOhm
Magnetics	T_1	PC44-PQ50/50 (TDK) Np:Ns = 15:7, L_m = 500 μH, L_k = 3.5 μH
	T_2	PC44-PQ50/50 (TDK) Np:Ns = 14:10, L_m = 500 μH, L_k = 3.5 μH
	L_1, L_2	PC44-PQ35/35 (TDK) L = 30 μH
Capacitors	C_1	B43647A5567M05 (4ea) 450 V/560 μF
	C_2	MKP1848C62580JP4 (3ea) 800 V/25 μF
MCU		TMS320F28384S

during high-power three-phase operation, where the regulated power is significantly reduced.

D. Design of Passive Components

The isolation stage of the proposed converter employs the DCX-SRC and operates at a load-independent point, rendering the design of the resonant components L_m, L_r, and C_r is depend on selected resonant frequency. L_m and L_r are derived from the

TABLE VI
COMPARISON OF SINGLE-PHASE AND THREE-PHASE COMPATIBLE OBC

	Proposed Sigma Converter	[6]	[31]	[32]
DC–DC topology	3Φ: Sigma (IPOS) 1Φ: Sigma (IIOS)	3Φ: CLLLC 1Φ: CLLLC	3Φ: Two dc–dc (IPOP) 1Φ: Two dc–dc (ISOP)	3Φ: Two dc–dc (IPOP) 1Φ: Two dc–dc (ISOP)
Switching frequency	180 kHz	100 kHz	No E-cap	No E-cap
Power rating	3Φ: 11 kW 1Φ: 7.36 kW	3Φ: 11 kW 1Φ: 6 kW	3Φ: 22 kW 1Φ: 19.2 kW	3Φ: 22 kW 1Φ: 7.36 kW
Grid voltage	3Φ: 380 V 1Φ: 220 V	3Φ: 380 V 1Φ: 220 V	3Φ: 400 V 1Φ: 230/240 V	3Φ: 400V 1Φ: 230 V
Battery voltage	250–450 V	240–500 V	No E-cap	200-450 V
DC–DC switch count	16	8	? (estimated at 16)	16
Switch utilization factor	0.1366	0.1410	No E-cap	No E-cap
Peak efficiency	98.12% (only dc–dc)	96.5%	No E-cap	94%
$V_{DC,Link}$	3Φ: 600–720 V 1Φ: 400 V	3Φ: 580–700 V 1Φ: 390–500 V	3Φ: 750 V 1Φ: 375 V	3Φ: No E-cap 1Φ: 350–400 V
$V_{E\text{-}cap}$	400 V (1 p.u.)	700V (2 p.u.)	375 V (1 p.u.)	Film cap with PD circuit
$C_{E\text{-}cap}$	2.24 mF (1 p.u.)	? (estimated at 1 p.u.)	2.7 mF (1 p.u.)	
E-cap volume (Assuming same capacitors/ 450 V/560 μF)	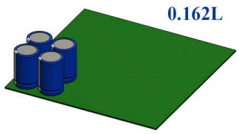	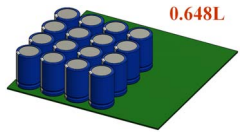	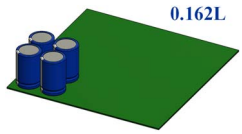	No E-cap

L_m and L_k values obtained during transformer fabrication, while C_r is designed considering the witching frequency

$$C_r = \frac{1}{L_r \cdot (2\pi \cdot f_{sw})^2}. \tag{26}$$

To determine the inductances L_1, L_2 of the buck–boost converter, it is first necessary to calculate the energy required for ZVS turn-ON. The required current can be obtained as follows, where C_{oss} denotes the output capacitance of switches S_5 and S_6, t_{dead} represents the dead time, and $V_{dc,Link}$ is the maximum dc-link voltage.

$$I_{ZVS} > \frac{2C_{oss} \cdot V_{DC,Link}}{t_{dead}}. \tag{27}$$

The ZVS turn-ON conditions of the buck–boost converter switches S_5, S_6, S_9, and S_{10} are provided in Table IV. It is assumed that the transformer magnetizing inductance L_m is very large, resulting in i_{Lr2} being zero at t_3 and t_7. Under these conditions, the turn-ON current of each switch, which corresponds to the buck–boost inductor current at each point, can be expressed as follows.

$$i_L(t) = \begin{cases} -I_{ZVS} & t = t_1 \\ -I_{ZVS} + \dfrac{V_{DC,Link} \cdot \phi}{L \cdot f_{sw}} & t = t_3 \\ -I_{ZVS} + \dfrac{V_{DC,Link} \cdot D - V_{bus}(D - \phi)}{L \cdot f_{sw}} & t = t_5 \\ -I_{ZVS} + \dfrac{V_{DC,Link} \cdot D - V_{bus}(1 - \phi)}{L \cdot f_{sw}} & t = t_7. \end{cases} \tag{28}$$

As shown in Fig. 5, $i_{L,t1}$ and $i_{L,t7}$ are always equal, and $i_{L,t5}$ is always greater than $i_{L,t3}$. Therefore, achieving $i_{L,t1} < 0$ and $i_{L,t3} > 0$ ensures ZVS turn-ON for all switches. The required inductance can thus be expressed as follows. The phase ϕ is set to the minimum duty cycle value under the given specifications [26]

$$L < \frac{V_{DC,Link} \cdot \phi}{I_{ZVS} \cdot f_{sw}}. \tag{29}$$

V. EXPERIMENTAL RESULTS

In order to verify the proposed sigma converter for single- and three-phase compatible OBC, an 11kW laboratory prototype was built according to the specifications given in Table VI. The photograph of the prototype is presented in Fig. 11, and the key components used are detailed in Table 5. Fig. 12 illustrates the experimental waveforms for various battery voltages in both single-phase and three-phase modes. Fig. 12(a) and 12(b) show the operational waveforms when the battery voltage is 250 and 450 V, respectively, in single-phase operation. It can be observed from the i_{Lr1} and i_{Lr2} waveforms that all switches on the primary and secondary sides of DCX1 and DCX2 achieve soft-switching. Fig. 12(c) and 12(d) show the waveforms for three-phase operation when the battery voltage is 250 and 450 V, respectively. The buck–boost filter inductor current i_{Lf2} and the primary currents of DCX i_{Lr1} and i_{Lr2} confirm that all switches on the primary side achieve ZVS turn-ON, and the secondary switches achieve ZCS turn-ON and turn-OFF. The measured efficiencies of the proposed sigma converter for various battery voltages are presented in Fig. 13. As shown in Fig. 13(a), a peak efficiency of 98.12% is achieved at 450 V during single-phase charging. In three-phase operation, the peak efficiency is 97.82% at a battery voltage of 330V, as depicted in Fig. 13(b). Table VI compares the proposed sigma-type dc–dc converter with dc–dc converters used in single- and

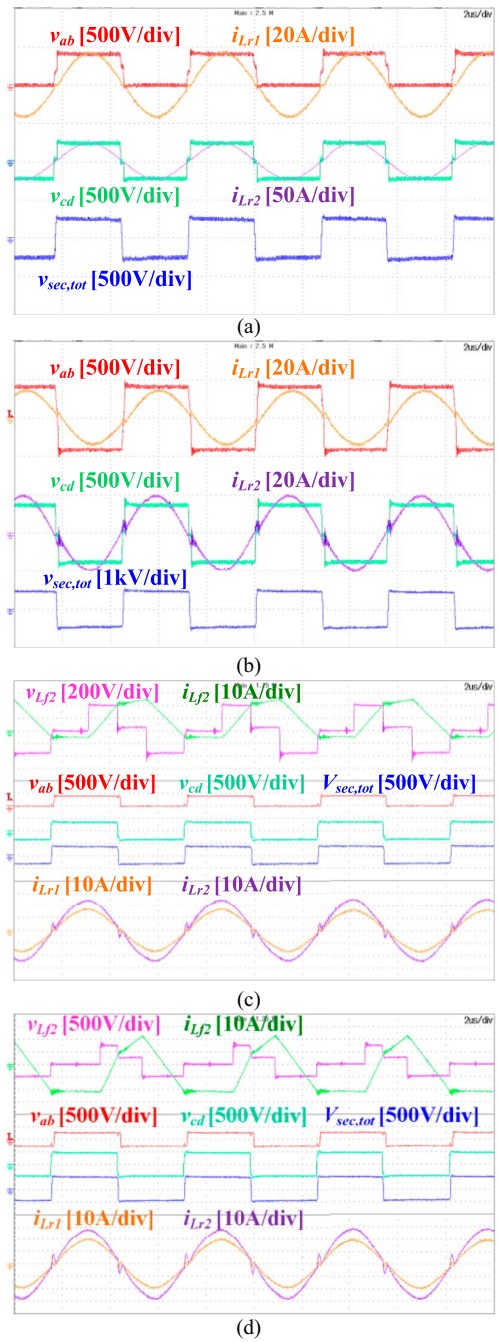

Fig. 12. Experimental waveforms of the converter. (a) Single-phase operation at $V_{bat} = 250$ V, $P_o = 5.26$ kW. (b) Single-phase operation at $V_{bat} = 450$ V, $P_o = 7.36$ kW full load condition. (c) Three-phase operation at $V_{bat} = 250$ V, $P_o = 7.86$ kW. (d) Three-phase operation at $V_{bat} = 450$ V, $P_o = 11$ kW full-load condition.

three-phase compatible OBC introduced in [6], [31], and [32]. The maximum dc-link voltage of the proposed converter is 720 V, similar to those of [6] and [31]. The E-cap voltage of [6] is high at 700 V, whereas the proposed converter achieves a lower rating of 400 V even during three-phase operation through relay structure, similar to [31]. The $C_{\text{E-cap}}$ capacitance of the proposed converter and [31] are equivalent, and although [6] does not specify this value, it is estimated to be comparable based on the specifications. The capacitance of the E-cap in the

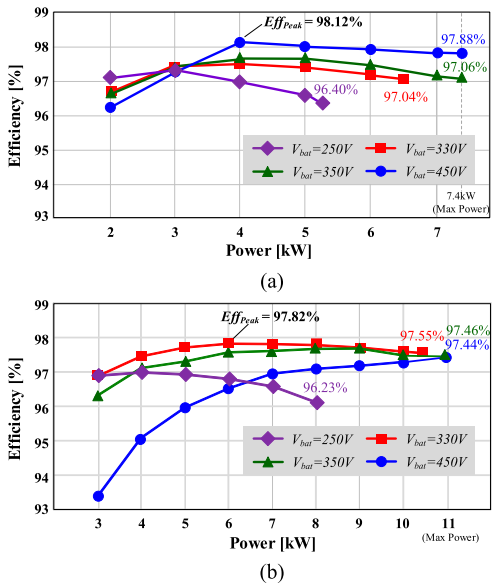

Fig. 13. Measured efficiencies of the proposed converter (Yokogawa WT-3000). (a) Single-phase operation. (b) Three-phase operation.

proposed converter is similar to that in [31]. Although not explicitly specified, the capacitance in [6] is estimated to be similar based on the provided specifications. This indicates that the E-cap volume of the proposed converter is half that of [6]. Since [31] only presents the concept of the dc–dc converter, no information or experimental results beyond the dc-link capacitor are available. While [6] uses only 8 switches for the dc–dc converter, the actual switch utilization factor is nearly similar to the proposed converter. Although it is difficult to make an exact comparison of the dc–dc converter efficiency, considering that the PFC efficiency is generally above 98%, it can be inferred that the proposed converter has higher efficiency than [32] and is similar to [6].

VI. Conclusion

In this article, a sigma-type dc–dc converter was proposed for single-phase and three-phase compatible OBC. The proposed relay structure allows for a reduction in the volume of electrolytic capacitors, which typically occupy large spaces during single- and three-phase operations. Additionally, the proposed structure achieved a peak efficiency of 98.12% in a single-phase grid by reducing conduction loss through an input-parallel configuration. In a three-phase system, it achieved a peak efficiency of 97.82% by reducing the regulated power. The proposed sigma converter achieved soft switching for all switches, including those in the unregulated converter, enabling high-efficiency operation at a high switching frequency of 180 kHz.

References

[1] A. Khaligh and M. D'Antonio, "Global trends in high-power on-board chargers for electric vehicles," *IEEE Trans. Veh. Technol.*, vol. 68, no. 4, pp. 3306–3324, Apr. 2019.

[2] "Global EV Outlook 2024," International Energy Agency, Apr. 2024. [Online]. Available https://iea.blob.core.windows.net/assets/a9e3544b-0b12-4e15-b407-65f5c8ce1b5f/GlobalEVOutlook2024.pdf

[3] I. Aghabali, J. Bauman, P. J. Kollmeyer, Y. Wang, B. Bilgin, and A. Emadi, "800-V electric vehicle powertrains: Review and analysis of benefits, challenges, and future trends," *IEEE Trans. Transport. Electrific.*, vol. 7, no. 3, pp. 927–948, Sep. 2021.
[4] Mark Kane, "Hyundai confirms 11 kW 3-phase on-board charger for Kona electric." InsideEVs, May 9, 2019. [Online]. Available: https://insideevs.com/news/348727/hyundai-3-phase-charger-kona-europe/
[5] H. Kim, J. Park, S. Kim, R. M. Hakim, H. Belkamel, and S. Choi, "A single-stage electrolytic capacitor-less EV charger with single- and three-phase compatibility," *IEEE Trans. Power Electron.*, vol. 37, no. 6, pp. 6780–6791, Jun. 2022.
[6] Y. P. Chan, Q. Li, B. Ponnuvelu, and R. T.-H. Li, "A single-/three-phase compatible V2G bidirectional on-board charger with reconfigurable structure," in *Proc. 11th Int. Conf. Power Electron. ECCE Asia (ICPE-ECCE Asia)*, Jeju Island, Republic of Korea, 2023, pp. 3151–3158.
[7] J. Schmenger, S. Endres, S. Zeltner, and M. März, "A 22 kW on-board charger for automotive applications based on a modular design," in *Proc. IEEE Conf. Energy Convers. (CENCON)*, Johor Bahru, Malaysia, 2014, pp. 1–6.
[8] G. Yang, E. Draugedalen, T. Sorsdahl, H. Liu, and R. Lindseth, "Design of high efficiency high power density 10.5 kW three phase on-board-charger for electric/hybrid Vehicles," in *Proc. PCIM Europe Int. Exhib. Conf. Power Electron., Intell. Motion, Renewable Energy Manage.*, Nuremberg, Germany, 2016, pp. 1–7.
[9] J. Lu et al., "A modular-designed three-phase high-efficiency high-power-density EV battery charger using dual/triple-phase-shift control," *IEEE Trans. Power Electron.*, vol. 33, no. 9, pp. 8091–8100, Sep. 2018.
[10] S. Rivera, S. Kouro, S. Vazquez, S. M. Goetz, R. Lizana, and E. Romero-Cadaval, "Electric vehicle charging infrastructure: From grid to battery," *IEEE Ind. Electron. Mag.*, vol. 15, no. 2, pp. 37–51, Jun. 2021.
[11] H. Kim, J. Park, S. Kim, R. M. Hakim, H. P. Kieu, and S. Choi, "Single-stage EV on-board charger with single- and three-phase grid compatibility," in *Proc. IEEE Appl. Power Electron. Conf. Expo. (APEC)*, Phoenix, AZ, USA, 2021, pp. 583–589.
[12] B. P. Do, M. Gerado Geda, J. Yun, K. Kang, S. Lee, and S. Choi, "Single-phase and three-phase compatible single stage OBC with 6-switches secondary side," in *Proc. IEEE 10th Int. Power Electron. Motion Control Conf. (IPEMC-ECCE Asia)*, Chengdu, China, 2024, pp. 1908–1912.
[13] H. Zhu, S. Hu, M. Tahir, Y. Bai, and X. Wu, "CLLC modeling and control in V2G mode to mitigate double-line frequency current for high-power density on-board charger," *IEEE Trans. Emerg. Sel. Topics Power Electron.*, vol. 12, no. 1, pp. 219–230, Feb. 2024.
[14] Z. Liu, B. Li, F. C. Lee, and Q. Li, "High-efficiency high-density critical mode rectifier/inverter for WBG-device-based on-board charger," *IEEE Trans. Ind. Electron.*, vol. 64, no. 11, pp. 9114–9123, Nov. 2017.
[15] B. Li, Q. Li, F. C. Lee, Z. Liu, and Y. Yang, "A high-efficiency high-density wide-bandgap device-based bidirectional on-board charger," *IEEE Trans. Emerg. Sel. Topics Power Electron.*, vol. 6, no. 3, pp. 1627–1636, Sep. 2018.
[16] M. Sameh Abdelmomen, I. Abdelsalam, and M. S. Hamad, "Two-stage single-phase EV on-board charger based on interleaved bridgeless AC–DC converter," in *Proc. 5th Int. Youth Conf. Radio Electron., Elect. Power Eng. (REEPE)*, Moscow, Russian Federation, 2023, pp. 1–6.
[17] J. C. Rodriguez, "An 11-kW bidirectional on-board charger with highly integrated SiC-cascode technology," in *Proc. IEEE Power Energy Conf. Illinois (PECI)*, Urbana, IL, USA, 2024, pp. 1–5.
[18] S. Choi, "Power converter technology for xEV-current status and challenge," in *Presentation at the Plenary Session, Proc. IEEE 9th Int. Power Electron. Motion Control Conf. (IPEMC-ECCE Asia)*, Nanjing, China, 2020, p. 19.
[19] M. Xu, Y. Liu, J. Sun, and F. C. Lee, "Σ/sigma DC/DC conversion for computing and telecom applications," in *Proc. IEEE Power Electron. Spec. Conf.*, Rhodes, Greece, 2008, pp. 1190–1195.
[20] X. Wu, H. Chen and Z. Qian, "1-MHz LLC resonant DC transformer (DCX) with regulating capability," *IEEE Trans. Ind. Electron.*, vol. 63, no. 5, pp. 2904–2912, May 2016.
[21] M. H. Ahmed, C. Fei, F. C. Lee, and Q. Li, "Single-stage high-efficiency 48/1 V sigma converter with integrated magnetics," *IEEE Trans Actions Ind. Electron.*, vol. 67, no. 1, pp. 192–202, Jan. 2020.
[22] Y. Cao et al., "Design and implementation of high-density isolated bi-directional soft-switching resonant DC–DC converter with partial power processing," in *Proc. IEEE Appl. Power Electron. Conf. Expo. (APEC)*, Phoenix, AZ, USA, 2021. pp. 640–646.
[23] M. ElMenshawy and A. Massoud, "Modular isolated DC–DC converters for ultra-fast EV chargers: A generalized modeling and control approach," *Energies*, vol. 13, no. 10, 2020, Art. no. 2540. [Online]. Available: https://www.mdpi.com/1996-1073/13/10/2540/
[24] X. Li, M. Zhu, M. Su, J. Ma, Y. Li, and X. Cai, "Input-independent and output-series connected modular DC–DC converter with intermodule power balancing units for MVdc integration of distributed PV," *IEEE Trans. Power Electron.*, vol. 35, no. 2, pp. 1622–1636, Feb. 2020.
[25] Q. Liu, Q. Qian, B. Ren, S. Xu, W. Sun, and L. Yang, "A two-stage buck–boost integrated LLC converter with extended ZVS range and reduced conduction loss for high-frequency and high-efficiency applications," *IEEE Trans. Emerg. Sel. Topics Power Electron.*, vol. 9, no. 1, pp. 727–743, Feb. 2021.
[26] Z. Wang, Z. Wu, T. Liu, C. Chen, and Y. Kang, "A high efficiency and high power density integrated two-stage DC–DC converter based on bipolar symmetric phase shift modulation strategy," *IEEE Trans. Power Electron.*, vol. 37, no. 4, pp. 4358–4373, Apr. 2022.
[27] Y. Bai, Y. Cao, V. Mitrovic, B. Fan, R. Burgos, and D. Boroyevich, "A simplified quadrangle current modulation for four-switched buck–boost converter (FSBB) with a novel small signal model," in *Proc. IEEE Appl. Power Electron. Conf. Expo. (APEC)*, Orlando, FL, USA, 2023, pp. 736–743.
[28] L. Xiao, X. Ruan, R. Dong, Y. Jiang, and T. Fu, "Analysis and modeling of a four-switch buck–boost converter with PWM plus phase-shift control," in *Proc. IEEE Appl. Power Electron. Conf. Expo. (APEC)*, Orlando, FL, USA, 2023, pp. 1307–1314.
[29] Q. Liu, Q. Qian, M. Zheng, S. Xu, W. Sun, and T. Wang, "An improved quadrangle control method for four-switch buck–boost converter with reduced loss and decoupling strategy," *IEEE Trans. Power Electron.*, vol. 36, no. 9, pp. 10827–10841, Sep. 2021.
[30] E. Gallo, F. Cvejić, G. Spiazzi, D. Biadene, and T. Caldognetto, "Average and small-signal model of the four-switch buck–boost converter under both duty-cycle and phase-shift modulation," in *Proc. IEEE Appl. Power Electron. Conf. Expo. (APEC)*, Orlando, FL, USA, 2023, pp. 1299–1306.
[31] P. Papamanolis, F. Krismer, and J. W. Kolar, "22 kW EV battery charger allowing full power delivery in 3-phase as well as l-phase operation," in *Proc. 10th Int. Conf. Power Electron. ECCE Asia (ICPE-ECCE Asia)*, Busan, Korea (South), 2019, pp. 1–8.
[32] K. Stengert, "On-board 22 kW fast charger "NLG6," in *Proc. World Electric Vehicle Symp. Exhib. (EVS27)*, Barcelona, Spain, 2013, pp. 1–11.

Jaehoon Kim was born in South Korea, in 1994. He received the B.S. degree from the Department of Energy and Electrical Engineering, Tech University of Korea, Siheung, South Korea and the M.S. degree from the Department of Electrical and Information Engineering, Seoul National University of Science and Technology (Seoul Tech), Seoul, South Korea, in 2016, and 2018, respectively, both in electrical engineering. He is currently working toward the Ph.D. degree in electrical and information engineering with Seoul Tech.

His research interests include power conversion technologies for renewable energy system and battery chargers for electrical vehicles.

Donghan Lee was born in South Korea, in 1993. He received the B.S. degree from the Department of Electrical Engineering, Korea National University of Transportation (KNUT), Chungju, South Korea, in 2016, and the M.S. degree from the Department of Electrical and Information Engineering, Seoul National University of Science and Technology (Seoul Tech), Seoul, South Korea, in 2020. He is currently working toward the Ph.D. degree with the Department of New and Renewable Energy Convergence, Seoul Tech.

His research interests include power conversion technologies for renewable energy system and battery chargers for electrical vehicles.

Chaeyoung Suk was born in South Korea, in 1995. She received the B.S. degree from the Department of Electrical Engineering, Soongsil University, in 2019, and the M.S. degree from the Department of Electrical and Information Engineering, Seoul National University of Science and Technology (Seoul Tech), Seoul, South Korea, in 2021.

Since 2021, she has been working as an Electric Power Conversion Engineer with LG Magna e-Powertrain, Incheon, South Korea.

Gibum Yu (Graduate Student Member, IEEE) received the B.S. and M.S. degrees in information and electrical engineering from Seoul National University of Science and Technology (Seoul Tech), Seoul, South Korea, in 2019 and 2021, respectively. He is currently working toward the Ph.D. degree in electrical engineering with the Center for Power Electronics Systems, Virginia Tech, Blacksburg, VA, USA.

His research interests include high-frequency soft-switching ac/dc converters, resonant converters, and power conversion in automotive and renewable energy applications.

Sewan Choi (Fellow, IEEE) received the Ph.D. degree in electrical engineering from Texas A&M University, College Station, TX, USA, in 1995.

In 1997, he joined the Department of Electrical and Information Engineering, Seoul National University of Science and Technology (Seoul Tech), Seoul, South Korea, where he is currently a Professor. From 1996 to 1997, he was a Principal Research Engineer with Samsung Electro-Mechanics Company, Suwon, South Korea. From 1985 to 1990, he was a Research Engineer with Daewoo Heavy Industries, Incheon, South Korea. He was the President of the Korean Institute of Power Electronics, Seoul, South Korea, in 2021. His research interests include high power density power conversion technologies for electric vehicles and renewable energy systems.

Dr. Choi served as a TPC Chair of ICPE2019-IEEE ECCE Asia held in Busan, South Korea and a Chairman of IEEE PELS Seoul section. He served as an Associate Editor of IEEE TRANSACTIONS ON POWER ELECTRONICS from 2006 to 2022. He was the recipient of the Prize Paper Award of IEEE Transactions on Power Electronics in 2022.